國立交通大學

電子工程學系電子研究所

碩士論文

應用於家用兩線電流檢測之軟性感應線圈

A Flexible Inductive Coil Tag for Household Two-Wire Current Sensing Applications

研 究 生：余松築

指導教授：鄭裕庭　教授

中 華 民 國 一 百 年 八 月

應用於家用兩線電流檢測之軟性感應線圈

A Flexible Inductive Coil Tag for Household Two-Wire Current Sensing Applications

研 究 生：余松築　　Student：Sung-Chu Yu

指導教授：鄭裕庭　　Advisor：Yu-Ting Cheng

國 立 交 通 大 學

電子工程學系電子研究所

碩 士 論 文

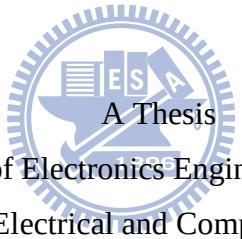

A Thesis

Submitted to Department of Electronics Engineering & Institute of Electronics

College of Electrical and Computer Engineering

National Chiao Tung University

in partial Fulfillment of the Requirements

for the Degree of

Master

in

Electronics Engineering

Aug. 2011

Hsinchu, Taiwan, Republic of China

中華民國一百年八月

應用於家用兩線電流檢測之軟性感應線圈

學生：余松築　　指導教授：鄭裕庭 教授

國立交通大學電子工程學系暨電子研究所碩士班

摘　　要

在此篇論文中，我們設計的軟性電流檢測線圈應用在家用雙線導線之電流監控，設計的方法分為空心線圈與加入導磁材料 NiFe 線圈，當感測器擺靠近一通有交流電源的雙線導線時，在感應線圈兩端將產生感應電動勢以供量測，並且使用實驗室先前發展的 SU-8 軟性基板技術使得感應線圈更貼近導線以達到更大的感應電壓輸出。感應線圈設計在一面積 5mmx10mm 的區域內，並且對於一個線圈數為九十圈的線圈而言提供了 68.5μV/A 的感測能力對於家用電 60Hz 的量測。

A Flexible Inductive Coil Tag for Household Two-Wire Current Sensing Applications

Student：Sung-Chu Yu　　Advisor：Dr. Yu-Ting Cheng

Department of Electronics Engineering & Institute of Electronics
National Chiao Tung University

Abstract

This thesis will demonstrate a flexible current sensor tag designed with inductive coils for sensing the current in the power cords of household-goods. The design methods for coils with air and NiFe (Ni71% Fe29%) magnetic material are compared. When the sensor is placed in proximity to a wire carrying AC electric current, a induced voltage in the inductive coils proportional to the current being measured and use a previously developed SU-8 flexible technology to reach better proximity to the power cord for maximizing induced voltage output. With three kind of different line widths and turns coil design in an area of 0.5 x 1 cm^2, for a 90-turns coil design, the sensor tag can provide a sensitivity of 68.5μV/A for detecting 60Hz electric current in the ampere regime.

誌　　謝

兩年果然撐一下就過了，轉眼間，碩士生涯就結束了，有苦有樂，苦的是實驗的迴圈，樂的是…身在 MIL。畢業了，當然首先感謝的是家人，在我在學的兩年裡，在心靈層面，給了我很大的支持，讓我可以心無旁騖的專注在實驗與課業上，感謝我的家人們！

在交大的兩年，很感謝我的指導教授－鄭裕庭老師，讓我了解如何從不同角度觀察事物，也讓我提早了解到社會的現實性。

接下來是感謝子元學長，每每都能對問題提出關鍵性的問答，能讓我好好的思考問題的根本，真是大恩不言謝。還有實驗室最強之男人-昌博，對所有我們的問題都有很犀利的見解，讓我們可以反覆的知道自己有多麼的渺小，戰鬥力有多強我就不再多做說明了，世人會見證這一切。還有要感謝冠銘學長，不管是在什麼時候都很熱心的幫助我們，幫我們渡過了許許多多的危機，還帶我們吃了很多好吃的東西(學長果然就是學長~~)，也希望三位學長能快點畢業。

另外還要感謝三位學弟睏寶，洋蔥跟展志平日裡常常幫我忙，雖然平常裡也滿機車的就是了，看到三位學弟比起我去年時更認真更努力，雖然跟畢業時間應該也是沒什麼關西，不過我覺得能有一起努力的伙伴在這碩士生涯裡，這一路上也不算寂寞了，當然跟博班比起來都算小咖拉~~~

最後，還有要感謝的人實在是太多了(系辦小姐，材料所小馬..等等)，也都祝你們順順利利。

Contents

摘要…… i
Abstract…… ii
致謝…… iii
Content…… iv
Figure Captions…… v
Table Captions…… vii

Chapter 1 Introduction **1**
Chapter 2 Principle And Design **3**
Chapter 3 Sensor Fabrication **8**
Chapter 4 Result and Discussion **13**
Chapter 5 Conclusion **22**
Reference **23**
Vita **25**

Figure Captions

Chapter1

Figure 1-1. The induced loop of Faraday current sensor……..…….1

Chapter 2

Figure 2-1. (a) The geometry of 1.25mm^2/2C power cord and (b) the simulation of magnetic flux distribution on 2C power cord at 1A, 60Hz input current…….3

Figure 2-2. The simulation of vertical magnetic flux distribution on 2C power cord……6

Figure 2-3. Cross section of Inductive Coil and power cord……6

Figure 2-4. The simulation of induced voltage versus coil turns……..6

Figure 2-5. The simulation and theory determine of induced voltage versus input-current for air coils……...7

Chapter 3

Figure 3-1. illustrates the fabrication process of the SU-8 flexible current sensor……...…..9

Figure 3-2. The optical photographs of the flexible inductive coil tag fabrication (a) that before sacrificial Cr layer released and (b) released from the substrate (c) after released for inductive coil with NiFe attached to the cord….10

Figure 3-3. SEM photograph of as-fabricated on inductive coil (a)top view of 30-turns air coil (b) 30μm line width of 30-turns coil (c) 30-turns coil with NiFe array (d) 30-turns coil with NiFe membrane (e)NiFe array each side is 10μm...12

Chapter 4

Figure 4-1. The active low-pass filter circuit scheme on the lower left hand side and the transfer function whose circuit gain is 66dB in spice simulation and 66.9dB in measurement respectively……...13

Figure 4-2. The oscilloscope monitor shows (a) a sinusoidal wave while the sensor pastes on and (b) no signal output while the sensor takes up from the power cord with 3A, 60Hz current input. The inset of (b) shows the as-fabricated device…….....14
Figure 4-3. The simulation and theoretical calculation of the induced voltage versus input-current for the inductive tag ……...16
Figure 4-4. The theory determined of induced voltage versus calculated values with different gap distances (a)air coil (b)NiFe membrane coil (c)NiFe array coil……...18
Figure 4-5. Hysteresis loop of NiFe with applied magnetic field……...19

Table Captions

Chapter 4

Table.4-1.Compares the specifications of references……...20

Chapter 1 Introduction

Improving energy efficiency has become a worldwide government policy in determining a national technology development roadmap owing to natural resource deficiency and global climate warming. Deployment of demand-response (DR) electricity monitoring systems in residential areas to well manage and devise the electricity usage in residential areas is a cost-effective way to accomplish this goal. Electric current sensor is one of the key components in the system. An electric current sensor must be with the characteristics of low-cost, pervasive, and easy-implementation for household goods power monitoring system applications.

Previously, various current sensors including Hall effect, fluxgate, AMR, piezo-MEMS and soon have been developed [1-4]. Either the sensor, like Rogowski coil[5,6], must enclose a power cord with the removal of ground or neutral line not practical to the household electrical system, or the sensor, like piezoelectric-MEMS [7], must be fabricated with a complex packaging process not cost-effective for residential applications [4]. In this work, a low-cost and robust sensor tag closely fitted with the power cords of household appliances is (Fig. 1-1), therefore, developed for advancing electricity monitoring systems for widespread use. Previously, Chen et al. has derived an analytical model based on the proposed sensor tag concept [13]. This thesis will expand upon the theoretical models of this current sensor and demonstrate the tag made of SU-8. Detail fabrication as well as some measurements and simulation results of the SU-8 flexible structure with inductive coils for the sensor are included in the

thesis.

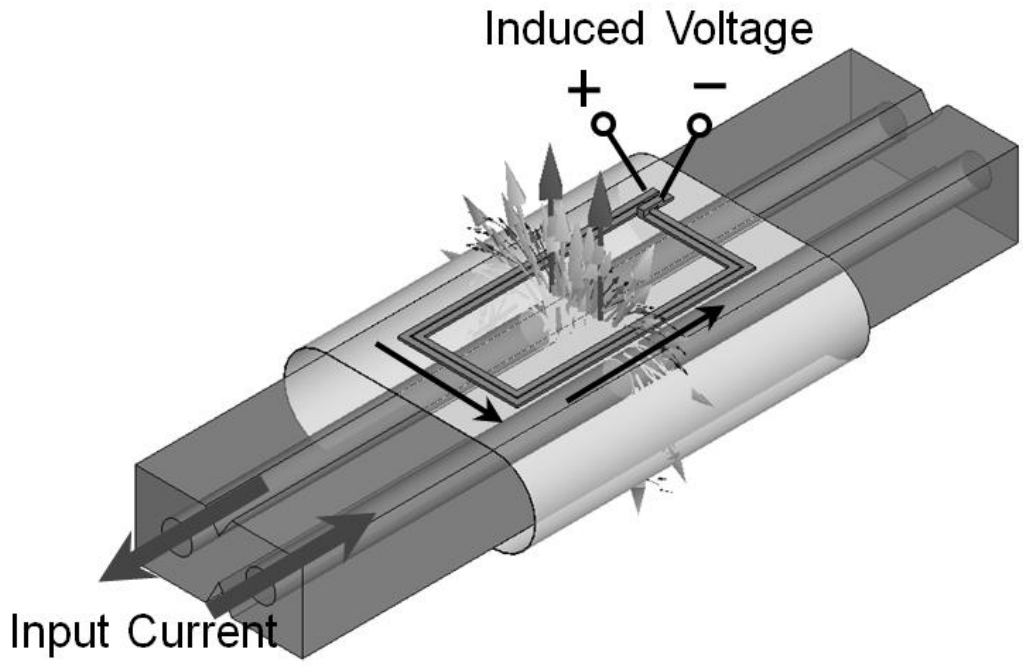

Figure 1-1. The induced loop of Faraday current sensor.

systems for widespread use. Previously, Chen et al. has derived an analytical model based on the proposed sensor tag concept [13]. This thesis will expand upon the theoretical models of this current sensor and demonstrate the tag made of SU-8. Detail fabrication as well as some measurements and simulation results of the SU-8 flexible structure with inductive coils for the sensor are included in the thesis.

Chapter 2 Principle And Design

Fig. 2-1. shows the scheme of 1.25mm^2/2C power cord (Fig. 2-1(a)) and the magnetic flux intensity distribution on the power cord with a 1A, 60Hz current input (Fig. 2-1(b)), respectively. According to Faraday's law of induction, the induced voltage which is proportional to the magnetic flux generated by the input current of the power cord can be described as follows [8]:

$$V_{in} = -\frac{d\Phi}{dt} = -N \cdot A \cdot \frac{dB}{dt} = -\mu_0 \cdot \mu_r \cdot N \cdot A \cdot \frac{dH}{dt} \quad (1)$$

Where Φ, A and N are the magnetic flux passing through the coil, the area and turns of the coil, respectively.

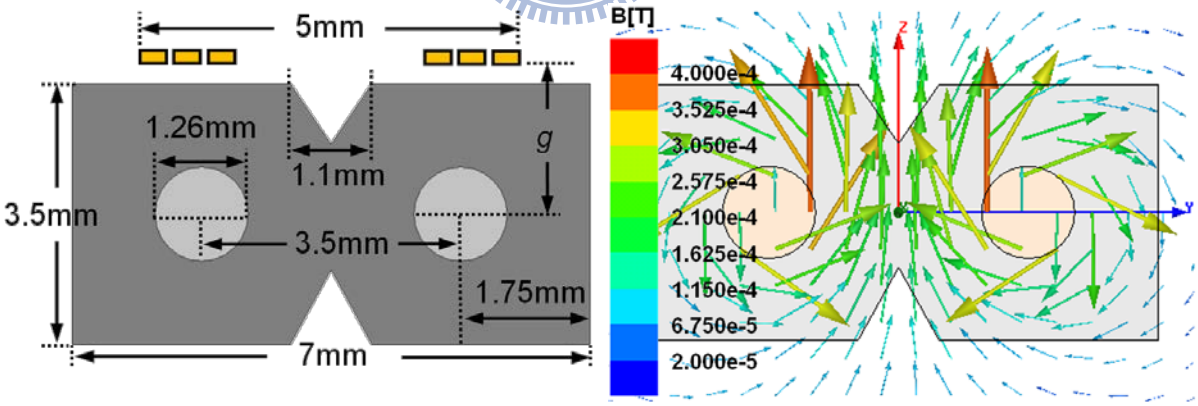

Figure 2-1. (a) The geometry of 1.25mm^2/2C power cord and (b) the simulation of magnetic flux distribution on 2C power cord at 1A, 60Hz input current.

The distribution indicates the largest vertical magnetic flux intensity to induce the highest open-loop voltage for current sensing exists on the top central

area of the power cord. Meanwhile, the flux intensity would decrease with the separation between the coil and this power cord (Fig. 2-2), therefore, in order to better proximity to the power cord in the fabricated process used previously developed SU-8 flexible technology [9]. Fig. 2-3 shows the geometry of power cord and inductive coils. According to Faraday's law of induction, the case induced voltage can be further derived from (1) as follows [13]:

$$\Phi_n = \int \vec{B} \cdot d\vec{A} = \frac{\mu_0 \mu_r I \cos \omega t}{\pi} c_n \int_{a_n}^{b_n} \frac{x}{x^2 + g^2} dx \tag{2}$$

$$V_{in} = -\sum_{n=1}^{N} \frac{d\Phi_n}{dt} = \frac{\omega \mu_0 \mu_r I \sin \omega t}{2\pi} \sum_{n=1}^{N} c_n \ln\left(\frac{b_n^2 + g^2}{a_n^2 + g^2} \right) \tag{3}$$

$$a_n = \frac{d}{2} - \frac{1}{2}\left[w_c - 2n \cdot w_d - 2(n-1) \cdot w_s \right] \tag{4}$$

$$b_n = \frac{d}{2} + \frac{1}{2}\left[w_c - 2n \cdot w_d - 2(n-1) \cdot w_s \right] \tag{5}$$

$$c_n = L - 2n \cdot w_d - 2(n-1) \cdot w_s \tag{6}$$

Where Φ_n = Magnetic flux of each turn

$I \cos(wt)$ = Current in the two-wire vary sinusoidally with time

a_n = Coil edge (Left) of each turn

b_n = Coil edge (Right) of each turn

c_n = Coil length of each turn

w_d = Line width

w_c = Coil width

w_s = Line Spacing

g = Total gap distance

d = Source Distance

L = Coil Length

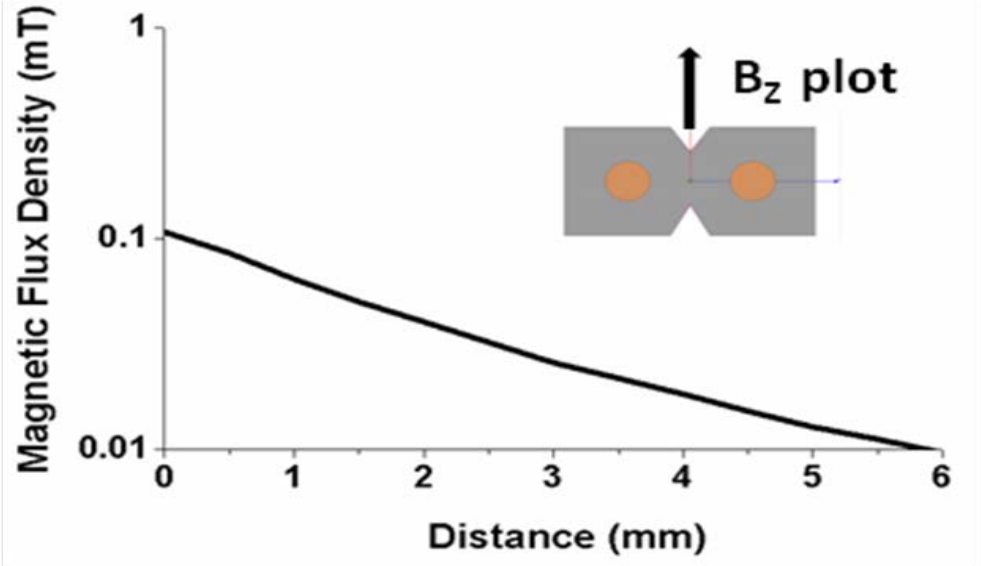

Figure 2-2. The simulation of vertical magnetic flux distribution on 2C power cord.

Fig. 2-4 shows the induced voltage versus the coil turns of the sensor for sensing 1A, 60Hz current input in the 2C power cord based on the theoretical model. For a 30-turns coil with an area of 5mm x 10mm, 30μm in width, 30μm line-spacing and a distance of 35μm to the cord top, i.e. the flexible substrate

thickness (SU-8 (35μm)), the induced voltage is only several tens of μV/A at the

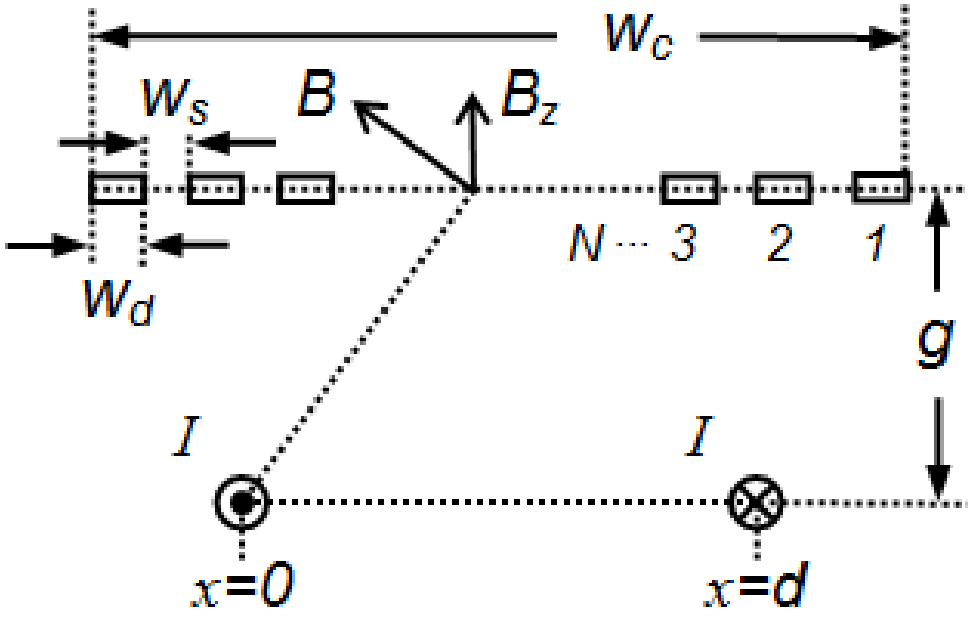

Figure 2-3. Cross section of Inductive Coil and power cord.

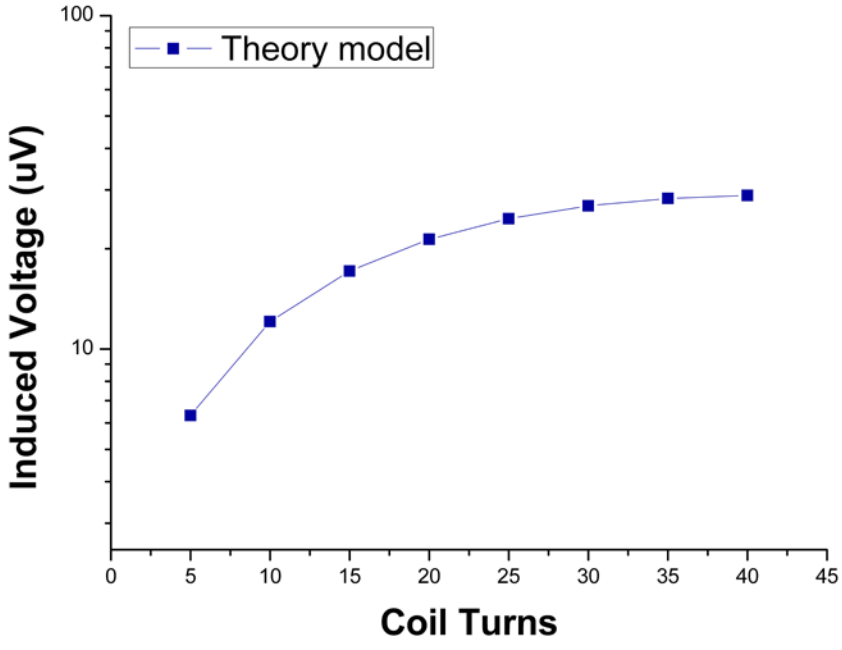

Figure 2-4. The simulation of induced voltage versus coil turns.

frequency 60Hz and will become saturated with the coil number. Fig. 2-5 shows

the comparison between the analytical model and Ansoft Maxwell simulation regarding the induced voltage of the sensor at different 60Hz current inputs in the 2C power cord. For the coil design with different turns, but the same line-spacing, i.e. 10μm, and the same area of 5mm x 10mm, the induced voltage of the sensing coils is proportional to the input current which can be well estimated by the derived model. Meanwhile, from equation (1), the induced voltage can be also enhanced as long as a magnetic core is introduced in the center of the inductive coil. The incorporation of a magnetic core can result in the increase of the total magnetic flux since the relative permeability (μ_r) becomes larger than 1. Thus, in the work, the inductive current sensor tag incorporated with a 4μm thick NiFe magnetic film as the core in the central of the coil is also fabricated to explore the feasibility in the device performance enhancement proposed by the model.

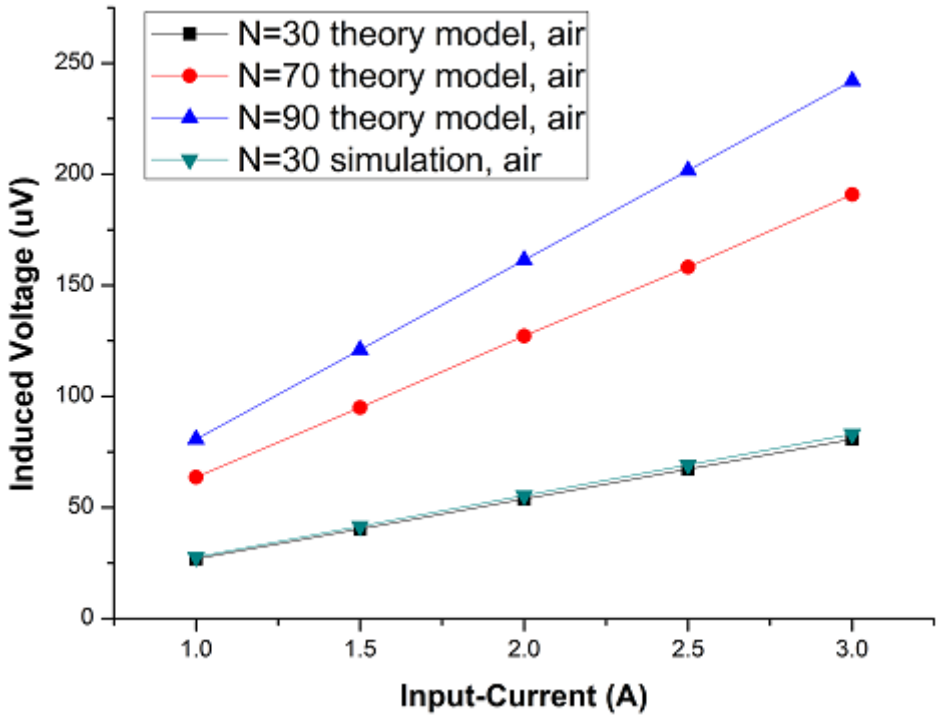

Figure 2-5. The simulation and theory determine of induced voltage versus input-current for air coils.

Chapter 3 Sensor Fabrication

The flexible inductive coils tag is fabricated using a previously developed SU-8 flexible technology [9], The flexible inductive coils of 30-turns, 70-turns and 90-turns are made of 5μm thick electroplated Cu. The coils of 30-turns, 70-turns and 90-turns are all designed in an area of 5mm x 10mm and 30μm, 15μm and 10μm in line width and 30μm, 10μm and 10μm in line-spacing, respectively.Fig. 3-1 illustrates the fabrication process of the SU-8 flexible inductive coil tags. A silicon substrate is first sputtered with 50nm thick Cr as a sacrificial layer as shown in Fig. 3-1 (a), followed by 35μm thick SU-8 spin coating as shown in Fig. 3-1 (b). After photo-patterning the SU-8 (Gersteltec Sarl GM 1060), a 50nm/100nm Ti/Cu seeding layer is deposited on the SU-8 as shown in Fig. 3-1(c) and followed by a photolithograph process using a 6μm thick AZ 4620 photoresist to patterned to define the region for coil fabrication of inductive sensor and electroplating an 5μm thick copper on that region as shown in Fig. 3-1 (d). After the first layer of 5μm thick Cu plating, another 6μm thick AZ 4620 is spun,patterned, and electroplating a 5μm thick copper for the via as shown in Fig. 3-1 (e), and sputtered with 150nm Cu seed layer for the via filling of Cu as shown in Fig. 3-1 (f). Fig. 3-1(g) shows another 6μm thick AZ 4620 is spun onto the plated structure,patterned, and plated with 5μm thick Cu to define air bridge after via filling.The AZ 4620 and seed layer are then removed using ACE, CR-7T as shows in Fig. 3-1(h). At the stage, the flexible inductive coil without a magnetic core is completed. For the case of the sensor tag with the NiFe magentci core, AZ4620 photoresist is spin-coated and patterned again to define the magnetic core region on the central area of the coil and used as a

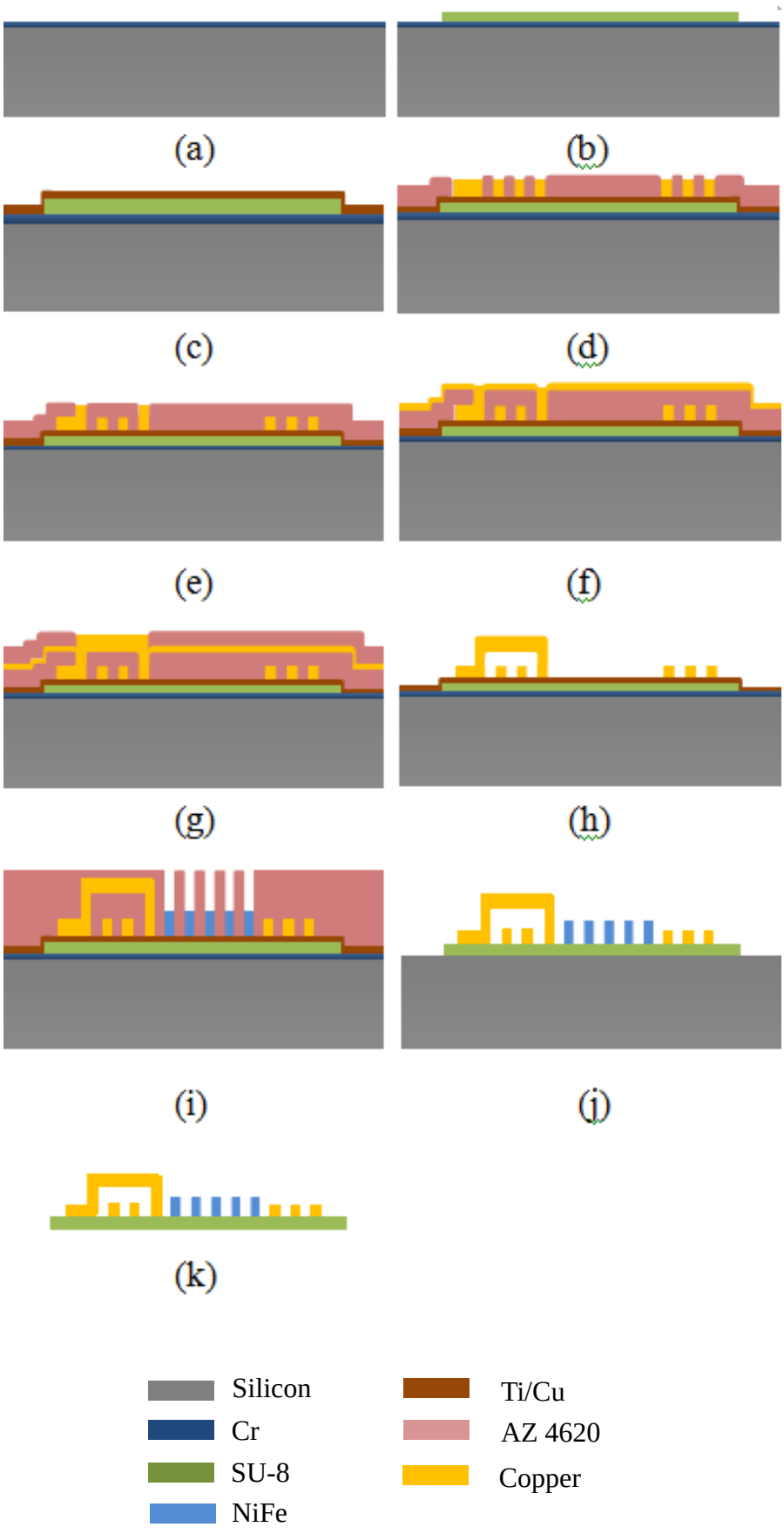

Figure 3-1. illustrates the fabrication process of the SU-8 flexible current sensor.

mold for electroplating a 4μm-thick NiFe layer as shows in Fig. 3-1(i), and AZ 4620 and Ti/Cu seed layer are then removed using ACE, CR-7T, BOE, respectively as shows in Fig. 3-1(j). At final, the SU-8 flexible inductive coil with NiFe core is released from the silicon substrate by dipping in a Cr etchant layer (H_2O:HCl=100:30) for the sacrificial layer removal as shows in Fig. 3-1(k).

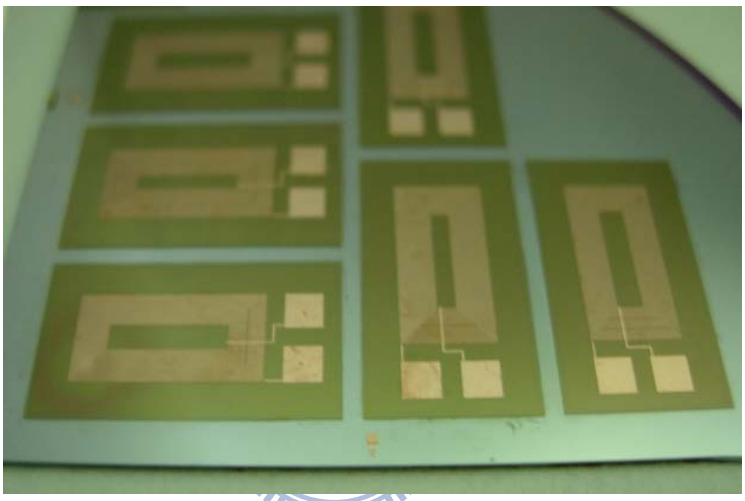

(a)

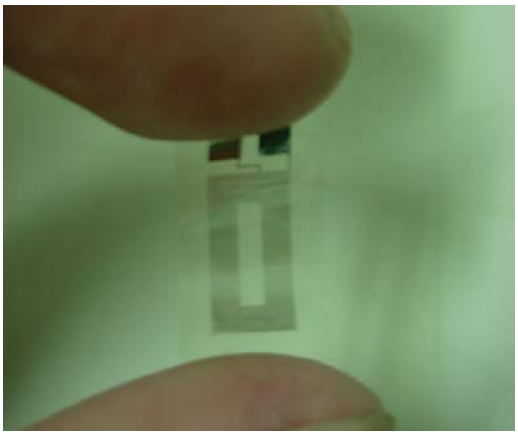

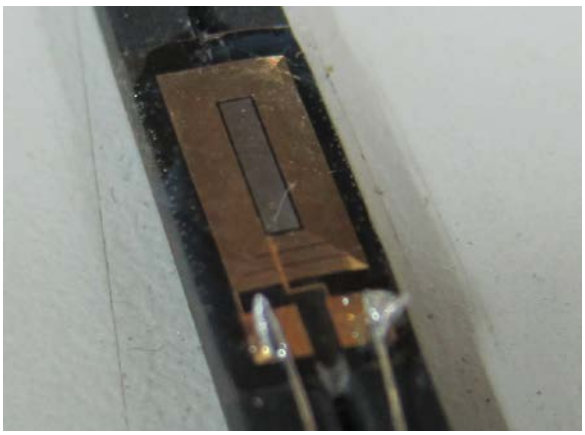

(b) (c)

Figure 3-2. The optical photographs of the flexible inductive coil tag fabrication (a) that before sacrificial Cr layer released and (b) released from the substrate (c) after released for inductive coil with NiFe attached to the cord

Fig. 3-2 shows the optical photographs of the as-fabricated sensor tag before (Fig. 3-2(a)) and after (Fig. 3-2(b)) the sacrificial Cr layer release and the tag with a magnetic core after (Fig. 3-2(c)) the sacrificial Cr layer release and then attached to the power cord, respectively. Fig. 3-3 shows the SEM image on the top of the 30-turns inductive coil (Fig. 3-3(a)) which is designed with 30μm in width and 30μm line-spacing (Fig. 3-3(b)). Fig. 3-3 (b) and (c) show the inductive coil tags with the cores of NiFe array and NiFe membrane, respectively. Fig. 3-3(e) shows the NiFe array core where the size of each element is 10x10 μm^2 and 10μm in spacing.

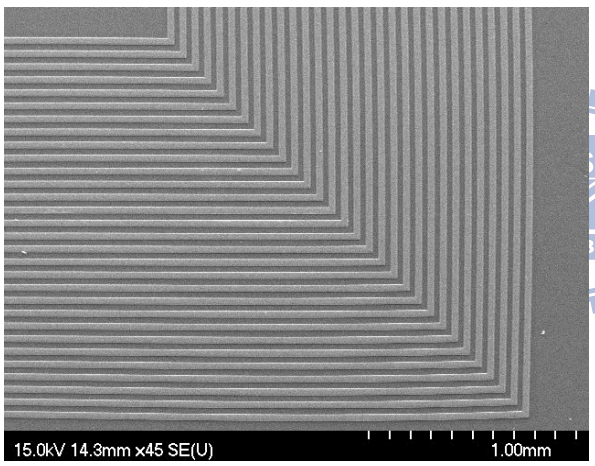

(a)

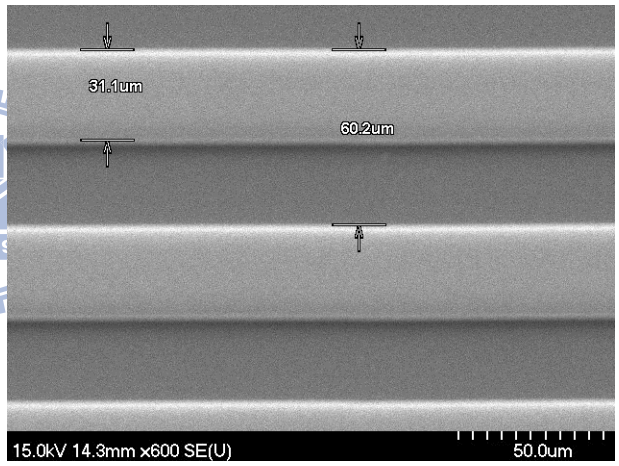

(b)

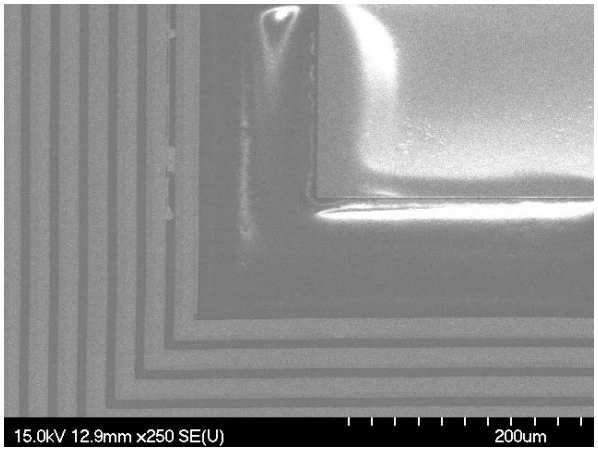

(c)

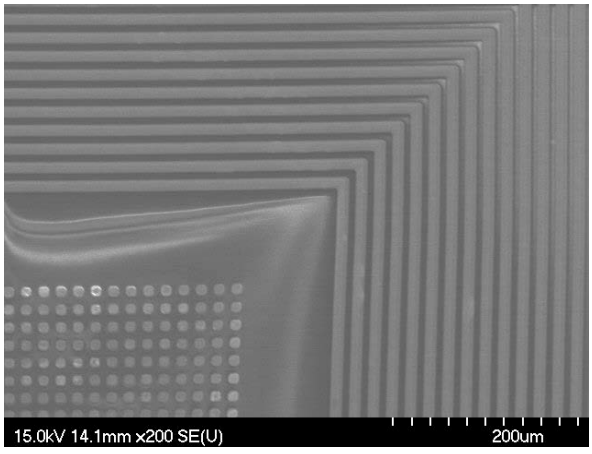

(d)

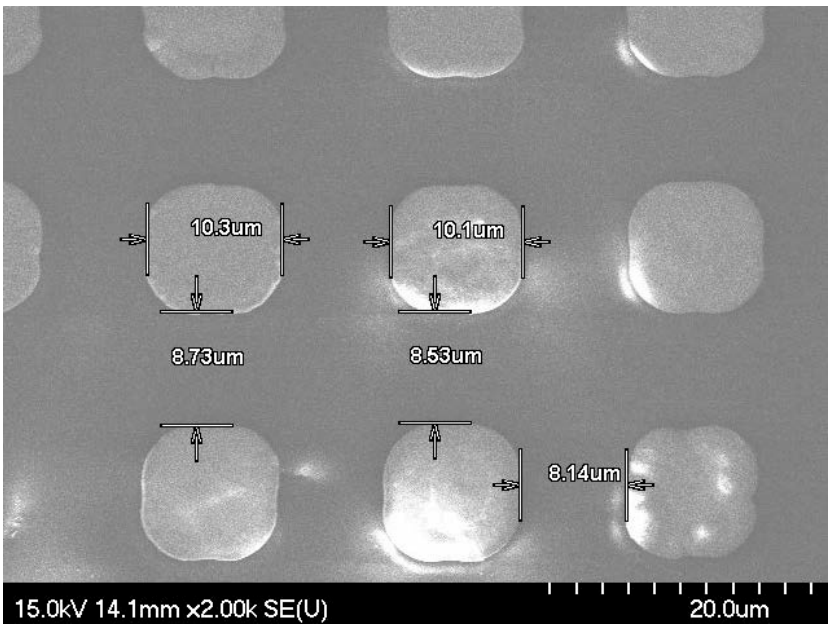

(e)

Figure 3-3. SEM photograph of as-fabricated on inductive coil (a)top view of 30-turns air coil (b) 30μm line width of 30-turns coil (c) 30-turns coil with NiFe array (d) 30-turns coil with NiFe membrane (e)NiFe array each side is 10μm

Chapter 4 Results And Discussion

According to the aforementioned analysis, the sensed signal is about several tens of μV/A which requires a signal amplifier for the electrical characterization of the flexible inductive coil. Fig. 4-1 shows an active low-pass filter circuit which is designed with 66.9dB gain resulted by the resistance ration of R_1(R_2) to R_3. In the work, 300 and 1MΩ variable resistors are chosen for a flat gain response in a frequency range of 45 to 100 Hz which is a typical range of the household AC power signals. The low noise operational amplifier, OP-27G (Texas Instruments Inc.), is used for the gain stage. The flexible inductive coil tag is then soldered with two metal wires connected to the circuit formed on a PCB.

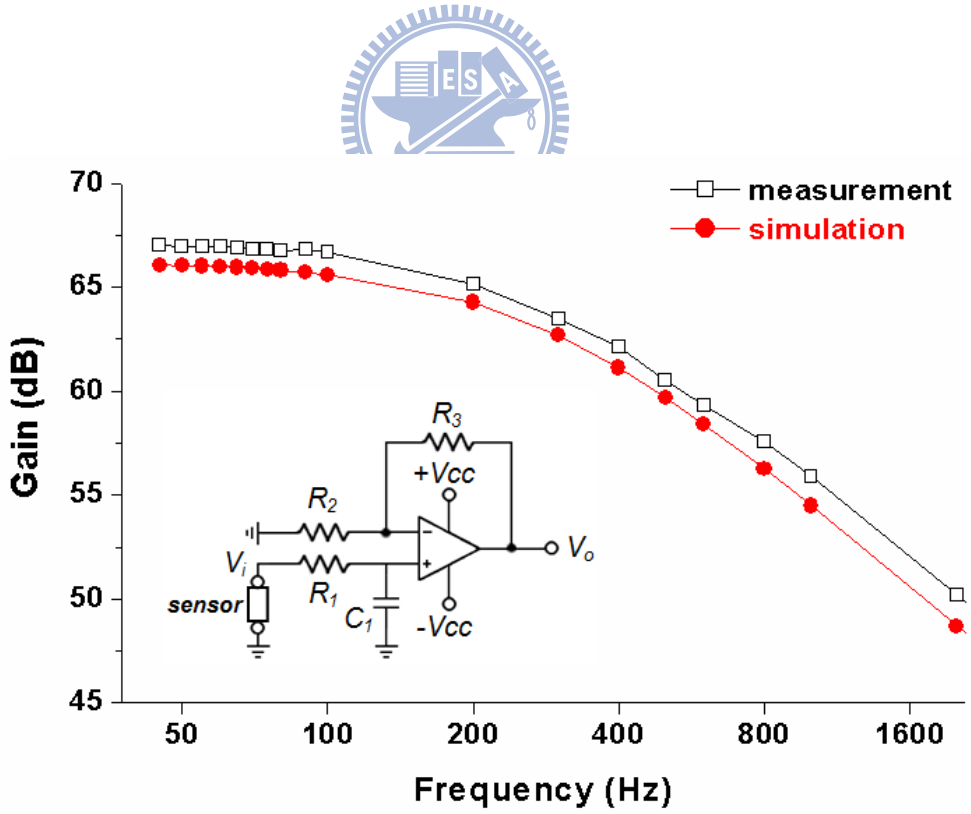

Figure 4-1. The active low-pass filter circuit scheme on the lower left hand side and the transfer function whose circuit gain is 66dB in spice simulation and 66.9dB in measurement respectively.

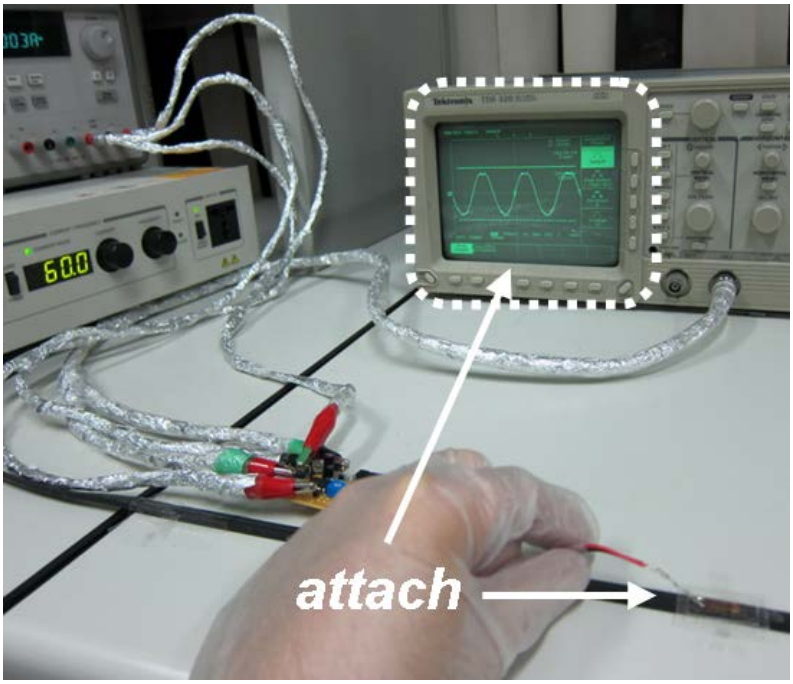

(a)

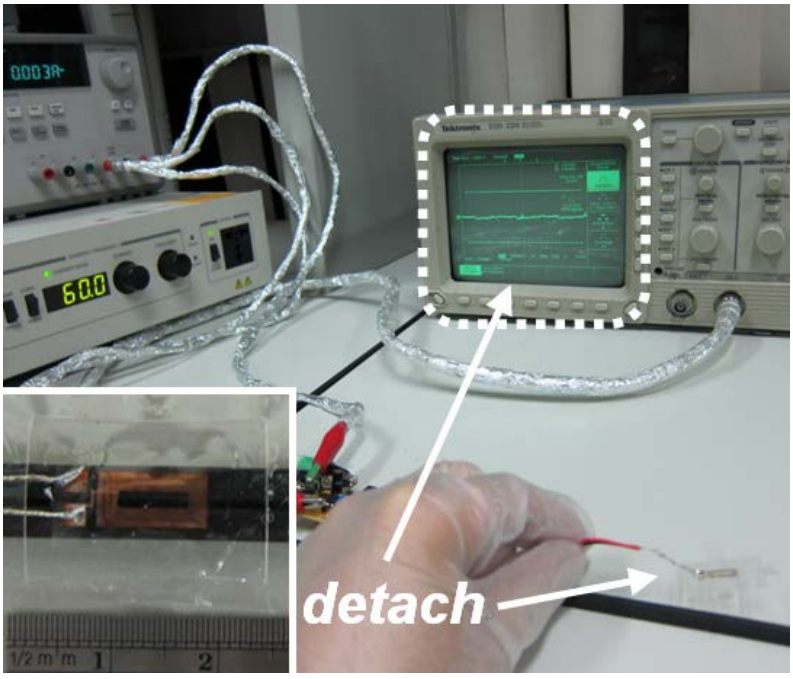

(b)

Figure 4-2. The oscilloscope monitor shows (a) a sinusoidal wave while the sensor pastes on and (b) no signal output while the sensor takes up from the power cord with 3A, 60Hz current input. The inset of (b) shows the as-fabricated device.

Fig. 4-2 shows the setup for the current sensing measurement. All feedthroughs are ground shielded to avoid electrical coupling and interference with the testing system. The senor tag shown in the inset of is attached to (Fig. 10a)/detached from (Fig. 10b) a 2C power cord loaded with the current source (ELGAR CW801M) with a 1A, 60Hz current output. When the tag is detached, the disappearance of the sensed signal in the oscilloscope validates the sensing mechanism of magnetic flux coupling and the feasibility of the flexible inductive coil tag for current sensing. Fig. 4-3 shows the measured voltage in the coils versus the input current in the cord. The data has been converted into the intrinsic signals without amplification. For 30/70/90-turns inductive coil tags, a linear relation of the induced voltage with the input current can be accomplished with the sensitivity of 23.2/55.5/68.5μV/A, respectively. While the as-fabricated tag is applied for detecting the 60Hz electrical current inputs in a 2C power cord in the ampere regime, it has been found that, instead of 26.9/63.6/80.7μV/A derived by the theory model, the average coupling efficiency of the 30/70/90-turns inductive coil tags is only 86/87/85% of the ideal values, respectively. Meanwhile, it is found that the induced voltage of the 30-turns inductive coils both with NiFe array and membrane cores can have the larger but similar sensitivity which is 26.3/25.6/μV/A, respectively. Since the total volume of the magnetic cores are quite different, the sensitivity difference between the coil with and without the magnetic core might not be caused by the magnetic flux enhancement. It could be attributed to poor attachment of the sensor tag to the power cord. Fig. 4-4 shows the measurement versus the theoretical calculation of the 30-turns inductive coil with different gap distances between the power cord and the coil. While the

gap is changed from the ideal value, i.e. 1.785mm, to 1.825mm and 1.815mm, the calculated data can well fit with the measurement results of the tags with the NiFe membrane and array cores, respectively. The ideal case is defined as the total thickness of the SU-8 layer and the coated insulator of the power cord. Although NiFe exhibits a large permeability μ_r, it should be taken into account that the resultant permeability of the core, μ_c, can be much lower than the material permeability due to the demagnetizing field effect which can be resolved by increase the aspect ratio of magnetic material [8]. In this work, the aspect ratios of the NiFe array and membrane cores are both less than 1, so the enhancement can be limited by the effect.

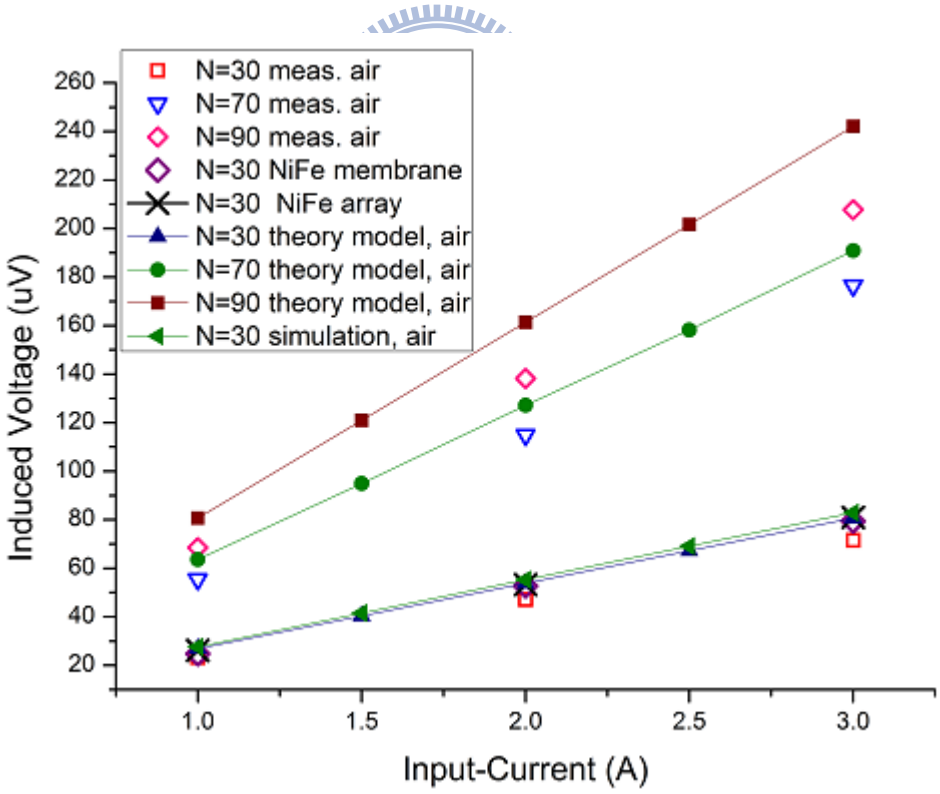

Figure 4-3. The simulation and theoretical calculation of the induced voltage versus input-current for the inductive tag .

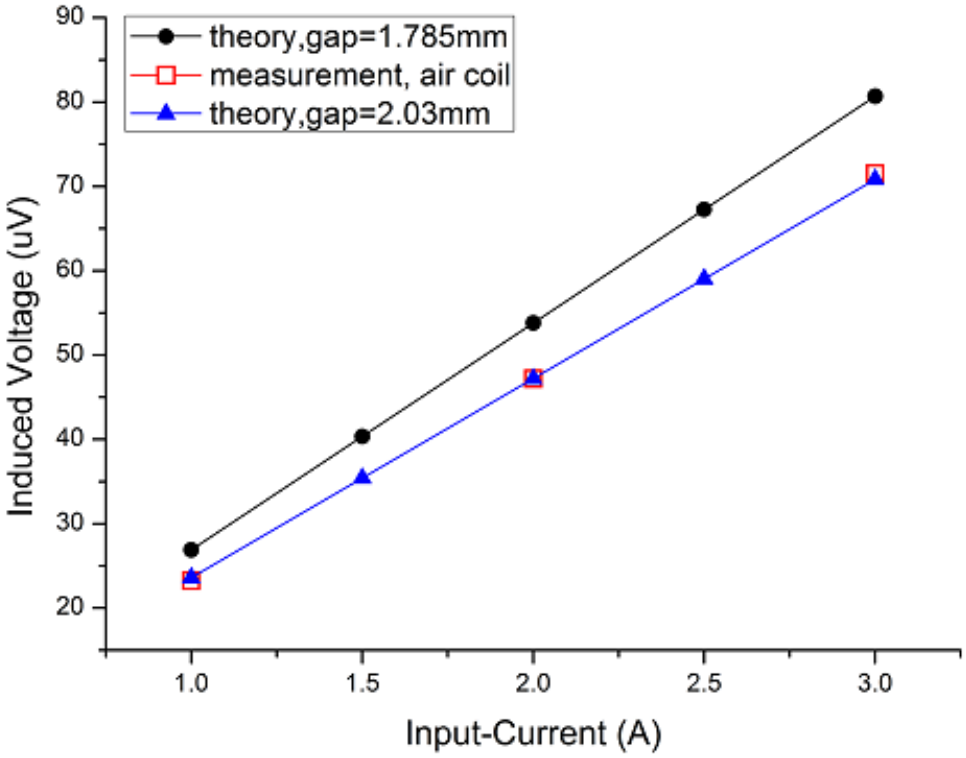
theory,gap=1.785mm
measurement, air coil
theory,gap=2.03mm
Induced Voltage (uV)
Input-Current (A)
90
80
70
60
50
40
30
20
1.0
1.5
2.0
2.5
3.0

(a)

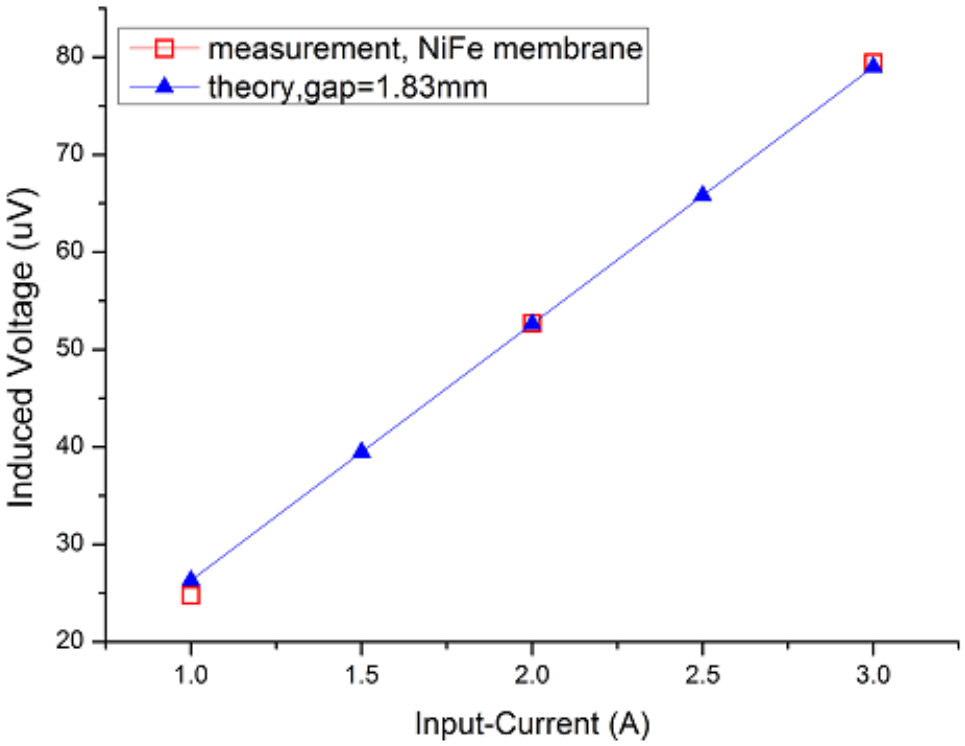
measurement, NiFe membrane
theory,gap=1.83mm
Induced Voltage (uV)
Input-Current (A)
80
70
60
50
40
30
20
1.0
1.5
2.0
2.5
3.0

(b)

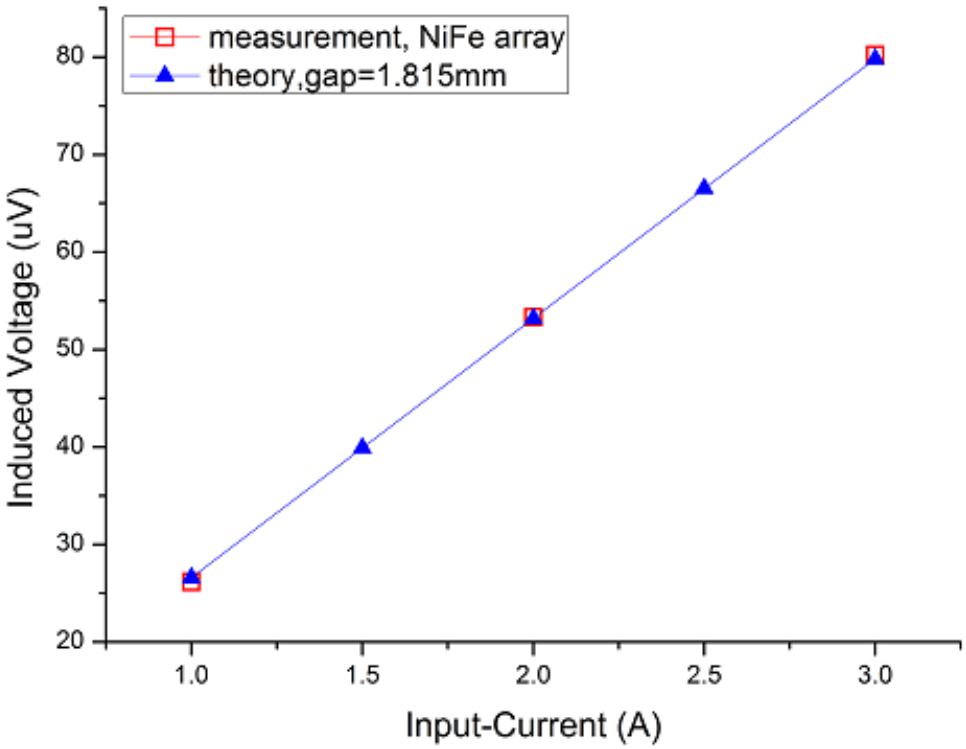

(c)

Figure 4-4. The theory determined of induced voltage versus calculated values with different gap distances (a)air coil (b)NiFe membrane coil (c)NiFe array coil

In fact, it can be further verified by the magnetic hysteresis measurement. Fig. 4-5 shows the superconducting quantum interference device (SQUID) measurements of the NiFe membrane with the fields whose directions are out of plane and in plane, respectively. From the slope of the M-H curve, the relative permeability can be calculated as follows:

$$\mu_r = 1 + 4\pi M / H_0 \tag{7}$$

where M is magnetization and H_0 is the applied magnetic field. The relative

permeability in our case is only about 1.4 which is quite small for the out-of-plane field. Negligible enhancement can be expected.

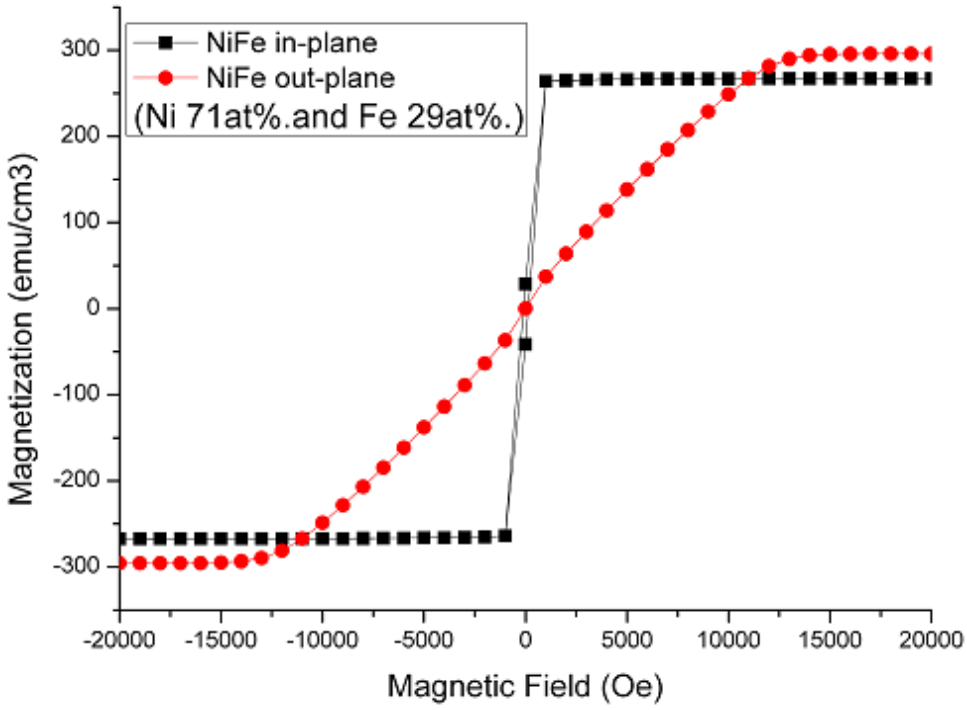

Figure 4-5. Hysteresis loop of NiFe with applied magnetic field

The sensitivity, in fact, decreases with the gap resulting in lower magnetic flux coupling. Although the flexible inductive coil tag is aimed to take the advantage of a good proximity effect on the current sensing, the connecting wires soldered to the tag would make the coil structure difficult in closely attaching to the power cord by manual control. Owing to the process characteristic of the flexible tag which is fully compatible with the previously developed SU-8 flexible technology, it is our belief that the sensitivity reduction problem can be further resolved by integrating the coil tag with a CMOS readout circuit chip with wireless data transmission function as a result of easy

implementation and good proximity.

TABLE.4-1

THE LIST OF CURRENT SENSORS

	Pernia *et al.*(1998)[10]	**Paprotny *et al.* (2010) [11]**
Sensor type	AMR	Piezoelectric
Sensor size	15.6*17.8*2mm	1*0.2mm
Circuit gain	80dB	40dB
Sensitivity*	80μV/A	0.87mV/A@60Hz
DC capable	Yes	No
Susceptible to DC magnetic field	Yes	Yes
Household two-wires application	Yes	Yes
Manufacturing process	Complicated	Complicated

*The results derived from the amplified data.

TABLE 4-1

THE LIST OF CURRENT SENSORS

	Schulz *et al.* (2010) [12]	***This work***
Sensor type	Rogowski coil	*Faraday induction*
Sensor size	2.5*4.5*0.45mm	*10*5mm*
Circuit gain	100dB	*66.9dB*
Sensitivity*	116nV/A-Hz	*80μV/A@60Hz*
DC capable	No	*No*
Susceptible to DC magnetic field	No	*No*
Household two-wires application	No	*Yes*
Manufacturing process	Simple	*Simple*

*The results derived from the amplified data.

The flexible sensor tag is compared with the state-of-the-art current sensors as shown in Table 4-1[10–12]. Basically, all of these sensors require amplified circuits, but the circuit specification of the presented one is not the most stringent in comparison with the others. Meanwhile, the coil size is much smaller than the wavelength of the background 60Hz EM wave (~5000 km) as a result of low antenna gain. The signal coupled from the environment EM field would be very extremely small.

In addition, the voltage induction of the presented air-coil sensor is irrelevant to any material properties. The sensor can be important because in contrary to other magnetic sensors, e.g. piezoelectric current sensor with a permanent magnet mounted, Hall sensor, it is not sensitive to DC component of magnetic field and environmental temperature. Thus, good proximity and stability indicate that the inductively sensing mechanism is feasible and the sensor can be prevailed for the applications of household electricity monitoring systems.

Chapter 5 Conclusion

A flexible inductive coil tag is demonstrated with the potential for the application to low-cost, reliable and pervasive DR electricity monitoring systems for residential power management. A physical model has been derived and verified for the coil design. According to the model, the sensitivity can be improved and determined immediately by reducing the metal width and increase the coil number simultaneously. Although the induced voltage will be saturated with the coil turns which is caused by less magnetic flux contribution from the inner coils closely to the central region, it can be resolved by incorporating a high aspect ratio ferromagnetic core since the sensitivity of the coil with magnetic material depends mostly on the dimensions and geometry of the core. Further experimental validation is required.

Reference

[1] P. Ripka, “Electric Current Sensor: a Review”, *Meas. Sci. Technol.*, Vol. 21, pp. 112001(23pp), 2010.

[2] S. Ziegler, R. C. Woodward, H. H. Iu, and L. J. Borle, “Current Sensing Techniques: A Review”, *IEEE Sens. J.*, Vol. 9, pp.354-376, 2009.

[3] W. F. Ray and C. R. Hewson, “High Performance Rogowski Current Transducers”, in *Proc. IEEE Ind. Appl. Conf.*, Rome, Italy, Oct. 8-12, 2000, Vol. 5, pp. 3083-3090.

[4] E. S. Leland, P. K. Wright, and R. M. White, “Design of a MEMS Passive, Proximity-Based AC Electric Current Sensor for Residential and Commercial Loads” in *Proc. PowerMEMS 2007*, Freiburg, Germany, Nov. 27-29, 2007, pp. 77-80.

[5]D. A. Ward and J. La T. Exon, “Using Rogowski coils for transient current measurements,” *Eng. Sci. Educ.* J., vol. 2, pp. 105–113, Jun. 1993.

[6] W. F. Ray and C. R. Hewson, “High performance Rogowski current transducers,” in *Proc. IEEE Ind. Appl. Conf.*, 2000, vol. 5, pp. 3083–3090.

[7]E. S. Leland, R. M. White, and P. K. Wright, “Design and fabrication of a MEMS AC electric current sensor,” *Adv. Sci. Technol.*, vol. 54, pp. 350–355, Sep. 2008.

[8]S. Tumanski, “Induction coil sensors – a review,” *Meas. Sci. Technol.*, vol. 18, pp. R31–R46, Jan. 2007.

[9] T. Y. Chao and Y. T. Cheng, “Wafer-Level Chip Scale Flexible Wireless Microsystem Fabrication,” will appear in *Proc. IEEE MEMS 2011*, Cancun, Mexico, Jan. 23-27, 2011.

[10]A. M. Penia, J. M. Lopera, M. J. Prieto, and F. Nuno, and S. Ollero, “Characteristics and Design of a Current Sensor Using Multilayer Co/Ni Structures,” in *Proc. APEC*, 1998, vol.1, pp. 414–419.

[11]I. Paprotny, E. Leland, C. Sherman, R. M. White, and P. K. Wright, “Self-powered MEMS sensor module for measuring electrical quantities in residential, commercial, distribution and transmission power systems,” in *Proc. IEEE ECCE*, Atlanta, USA, 2010, pp. 4159–4164.

[12]C. A. Schulz, S. Duchesne, D. Roger, and J. Vincent, “Short circuit current measurements between transformer sheets,” *IEEE Trans. Magn.*, vol. 46, pp. 536–539, Feb. 2010.

[13] Y. C. Chen, S. C. Yu, S. H. Cheng, and Y. T. Cheng, “A Flexible

Inductive Coil Tag for Household Two-Wire Current Sensing Applications," submitted to IEEE sensors Journal

Vita

姓　　名：余松築 (Sung-Chu Yu)

出生日期：中華民國七十六年一月二十一日

出 生 地：中壢市

E - mail： h2oduoljr@gmail.com

學　　歷：

國立內壢高級中學 (2002.9～2005.6)
(National Neili Senior High School)

國立中正大學物理學系 (2005.9～2009.6)
(Department of Physics, National Chung Cheng University)

國立交通大學電子工程所碩士班 (2009.9～2011.8)
(Department of Electronics Engineering & Institute of Electronics, Nation Chiao Tung University)